JOINT INSTITUTE FOR NUCLEAR RESEARCH

Veksler and Baldin Laboratory of High Energy Physics

FINAL REPORT ON THE START PROGRAMME

Optimization of the geometry of ETOF MPD end-of-flight time-of-flight detectors for use in the ACTS tracker

Supervisor: Vadim Andreevich Babkin

Student: Kirill Veretennikov, Russia
Moscow State University

Participation period:
July 05 – August 16,
Summer Session 2025

Dubna, 2025

Contents

Abstract

We adapted the geometry of the MPD Endcap time-of-flight detector (ETOF) in MPDRoot to the target configuration, enabling realistic *occupancy* estimates and subsequent track reconstruction in ACTS. The inner radial portion of each sector was shortened by removing 16 strips (from 64 to 48 per sector) with a corresponding recalculation of trapezoid dimensions and placement. The ETOF modules were moved from $Z = \pm 300$ cm to $Z = \pm 325$ cm; a `TGeo`/TEve (`CheckOverlaps`) scan found no overlaps. A macro to evaluate *occupancy* as a function of radius was implemented.

In addition, a laboratory prototype of an MRPC module (active area 6×12 cm, 5 gas gaps) was manufactured: glass cutting (thin ∼250 µm, high-voltage ∼500 µm), application of a resistive layer to the HV glass (resistance of order 10 MΩ), and design/printing of a frame on a photopolymer 3D printer. Sealing at the assembly stage was done with a sealant. Electrical tests and connection to readout electronics were not performed.

1 Introduction

1.1 The MPD detector

The Multi-Purpose Detector (MPD) is the main experimental detector of the NICA project under construction at the Joint Institute for Nuclear Research (JINR, Dubna). The extensive MPD physics program requires high-precision measurements. The detector used in this work, designed with modern advances in detection techniques and electronics, fully meets the stated objectives [1].

Figure 1 shows the detector layout as an axial cross section.

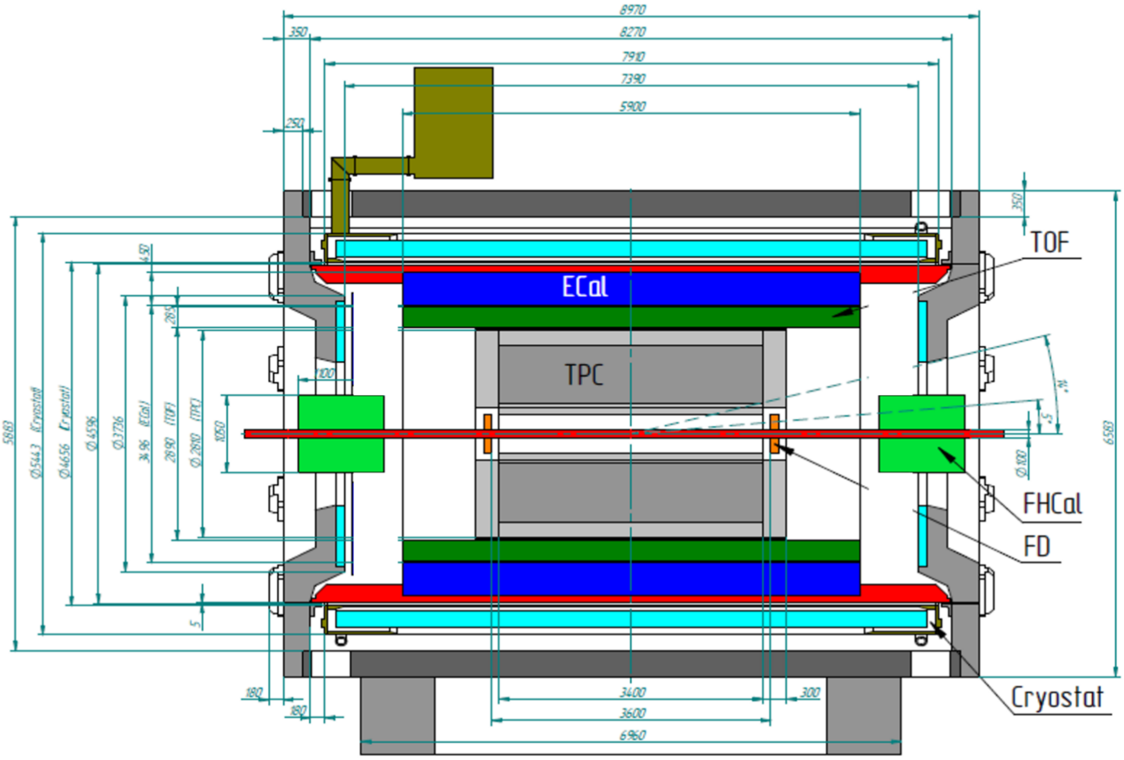

Figure 1: MPD layout with principal dimensions [1].

The detector is a cylinder with endcap sections arranged around the interaction region. MPD is a 4π spectrometer capable of registering hadrons, electrons, and photons produced in heavy-ion collisions [1].

The MPD construction is organized in two main stages:

Stage I includes the minimal set of subsystems sufficient for a full physics program in the energy range $\sqrt{s_{NN}} = 4{-}11$ GeV. This stage comprises the main subsystems: ITS, TPC, TOF, ECAL, ZDC, and the magnet system [1, 2, 3].

Stage II extends Stage I by adding further elements. In particular, it includes [4]:

- **ITS (Inner Tracking System)** — installation of a vertex silicon tracker;
- **FTS (Forward Tracking System)** — a forward tracking system based on sTGC (small-strip Thin Gap Chambers), enabling track reconstruction at large $|\eta|$;
- **ETOF (Endcap TOF)** — an endcap time-of-flight system designed to register particles emitted at small polar angles (large pseudorapidity, $1.54 \leqslant |\eta| \leqslant 2.04$). ETOF covers angles inaccessible to the barrel TOF system;

Including ETOF extends the PID pseudorapidity range and provides particle identification in the forward region (together with the forward tracker).

1.2 MPD physics

The MPD physics program covers a broad range of topics on the properties of strongly interacting matter formed in heavy-ion collisions. The main interest is the QCD phase diagram, especially at high baryon densities and moderate temperatures, which are not probed in other experiments (not reachable at LHC energies and only partially explored in the RHIC-BES program) [1]. MPD will enable systematic studies in the range $\sqrt{s_{NN}} = 4{-}11$ GeV, where the baryon chemical potential reaches $\mu_B \approx 300{-}800$ MeV, corresponding to the region of maximum baryon densities and a potential critical point of the QCD phase diagram [1, 5]. Each MPD subsystem plays an important role:

- TPC and ITS provide tracking information for trajectory reconstruction and primary/secondary vertex determination;
- TOF and ETOF provide time-of-flight, crucial for mass-based particle identification;
- ECAL is used to study electromagnetic processes;
- ZDC determines the collision centrality.

1.3 A Common Tracking Software

A Common Tracking Software (ACTS) [6, 7] is an open, modular tracking framework for high-energy physics experiments, derived from the ATLAS reconstruction toolchain and re-envisioned as a detector-agnostic library. ACTS provides common components for detector geometry and material description, magnetic-field modeling, particle propagation, track finding (seeding/CKF) and fitting (Kalman-filter variants, including adaptive and multi-vertex methods), as well as tools for alignment, simulation, and performance analysis [8, 6].

Decoupling algorithms from a specific detector implementation enables porting the same reconstruction across setups and configurations while reusing optimized C++ algorithms, vectorization, and multithreading. Adapters are available for I/O and visualization with ROOT and other tools. The framework is under active development [7].

In the context of this work, ACTS is treated as the *target* platform for subsequent track reconstruction in the MPD detector. The ETOF geometry adaptation in MPDRoot, overlap checks, and *occupancy* calculations were carried out as a preparatory step toward exporting the geometry into the ACTS surface representation and continuing the studies within that framework.

Thus, the geometry parameters and *occupancy* profiles obtained here provide the boundary conditions and input for configuring track reconstruction in ACTS at the next stage (ETOF transfer to ACTS, reconstruction validation, and further improvements in algorithm accuracy and robustness).

2 Project Goals

Goals:

- ▷ Adapt the ETOF geometry in MPDRoot to the planned configuration: shorten the inner part of the sector and reduce the number of strips from 64 to 48 per sector (with recalculation of dimensions and placement) to ensure proper pseudorapidity coverage.
- ▷ Move the ETOF modules from $Z = \pm 300$ cm to $Z = \pm 325$ cm to align with neighboring subsystems (avoid overlaps) and improve pseudorapidity coverage.
- ▷ Ensure correct assembly of the full MPD geometry, visualization, and overlap checks.
- ▷ Perform preliminary geometry tuning and implement occupancy vs. radius computation in the current MPDRoot setup with a view to porting the final configuration to the ACTS (A Common Tracking Software) geometry [6, 7].
- ▷ Develop a prototype of a *sealed MRPC*: design the frame, cut glass, apply a resistive layer, and assemble a multi-gap structure for further tests.

3 ETOF Geometry

3.1 MPDRoot geometry

The geometry is implemented with the ROOT/MPDRoot framework. The original ETOF geometry did not meet the updated requirements on channel count and placement, necessitating its adaptation. The work included:

- ▷ reducing the number of strips from 64 to 48 per sector by "trimming" the inner part (increasing the inner radius) with recalculation of trapezoid dimensions;
- ▷ shifting the ETOF modules along the Z axis from ±300 to ±325 cm;
- ▷ updating the software responsible for generating ETOF *points* and verifying the assembled geometry for overlaps.

Conceptual requirements for TOF/ETOF are summarized in [1, 9]; general information on software and geometry is available on the MPD website [10].

3.2 MRPC for TOF

The time-of-flight (TOF) system is based on MRPC technology, which provides excellent time resolution at moderate cost [1, 3]. An MRPC is a stack of alternating resistive glass plates and gas gaps. In an electric field, electrons produced by a traversing charged particle undergo avalanche multiplication [1]. The gas mixture is tuned for stable operation and minimal electron drift time. Signals are read out from both ends, allowing measurement of time-of-flight and the coordinate along the strip [11].

Barrel TOF. Surrounds the TPC and covers $|\eta| < 1.44$. A time resolution of about 50–60 ps enables effective $\pi/K/p$ separation [11].

ETOF. The endcap sections register particles at large pseudorapidity, $1.54 \leqslant |\eta| \leqslant 2.04$. The placement and dimensions of modules depend on the locations of other detectors, requiring a compact ETOF layout and careful cable management [9].

4 Geometry Implementation

The `MpdEtof` class implements the ETOF sensitive endcap detector within FairRoot:

1. marks ETOF sensitive volumes (strip gas gaps, $ActiveSV$) and handles particle traversal;
2. produces `MpdTofPoint` MC points at the exit of a sensitive volume with coordinates, momenta, time (ns), track length, and total energy deposition;
3. encodes the volume address (wheel, sector, gap, strip) in `detID` and adds the points to the event collection (`ETOFPoint`);
4. registers the collection in `FairRootManager` for writing to the ROOT output.

Geometry loading is performed by `ConstructGeometry()` from a pre-built ROOT file. The `MpdEtofGeo`/`MpdEtofGeoPar` classes place sensitive/passive volumes and store parameters in `FairRuntimeDb`. The actual volumes (trapezoids, frames, strips) are constructed in an external geometry macro (`MakeMPDROOT_ETOFv6_3()`), which `MpdEtof` then consumes.

Submodules are specified in `geometry_stage1.C`, where TPC, TOF, ETOF, Magnet, ZDC, etc., are listed and each detector is assigned its own geometry `.root` file:

```
FairDetector *etof = new MpdEtof("TOF_ENDCAP", kTRUE);
etof->SetGeometryFileName("etof_v5_1.root");
fRun->AddModule(etof);
```

The call `fRun->AddModule()` adds the detector to the global list of simulation modules so that during initialization (`fRun->Init()`) FairRoot creates the geometry, registers sensitive volumes, and ensures the handoff from the Geant4 tracker to the event data structures.

At the final stage, the `runMC.C` macro initializes the whole system (geometry, physics, input files) and starts the event loop. Thus each detector (including ETOF) operates as a standalone module connected to the FairRoot infrastructure via `fRun`.

5 ETOF Work and Modifications

5.1 Motivation for changes

Central heavy-ion collisions produce a large number of secondary particles, increasing the track density in the detector. This load is especially noticeable in endcap subsystems such as ETOF, where particles at large $|\eta|$ traverse sensitive elements at small polar angles—predominantly near the inner radius. In this region, a higher density of track intersections is observed.

Preliminary estimates indicate high track densities for pseudorapidity above 2, which leads to reduced reconstruction efficiency.

In the initial configuration, 64 strips per sector were foreseen. To reduce local hit density and ensure robust track reconstruction, the inner part of the sector was shortened—reducing the strip count to 48. In addition, the ETOF modules were shifted along the Z axis from ±300 to ±325 cm to align with mechanical constraints of the setup.

5.2 Applying corrections to ETOF

The target sector view is shown in Fig. 2. The first macro-generated geometry version is shown in Fig. 3. The initial parameters and required changes are listed below:

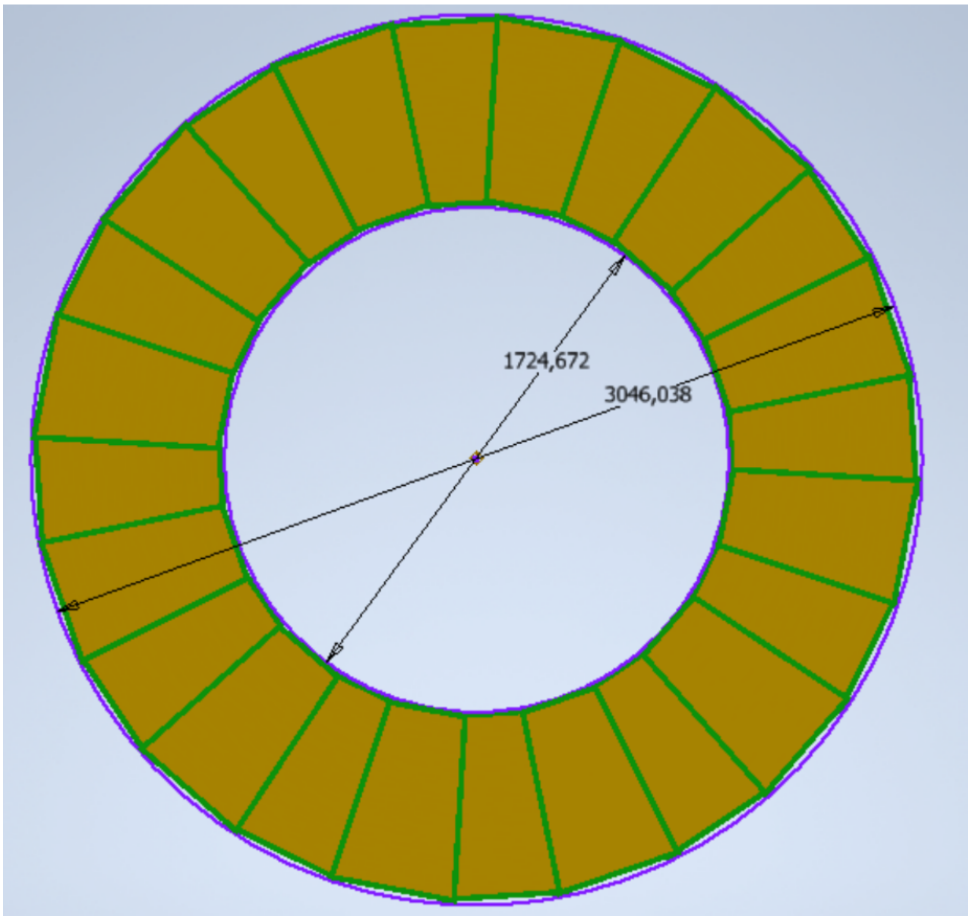

Figure 2: Target geometric representation of ETOF (reducing to 48 strips per layer).

Initial parameters (before modification).

```
const double innerTrdX1 = 18.936; // short base of the trapezoid (at small radius)
const double innerTrdX2 = 40.0;   // long base of the trapezoid (at large radius)
const double innerTrdY  = 80.0;   // trapezoid height (along the radius)

const double stripY = 1.25;       // radial pitch for one strip
const int    Nstrips = 64;        // strips per sector before modification
// Consistency check: 64 * 1.25 = 80 = innerTrdY
```

Required changes.

1. Reduce the strip count to $N_{\text{strips}} = 48$:

```
const int Nstrips = 48;
```

2. Decrease the trapezoid radial height to 60 cm (48 * 1.25):

```
const double innerTrdY = 60.0;
```

3. Recalculate the short base (`innerTrdX1`), since the inner part is “trimmed” by 20 cm from the original 80 cm:

```
const double dY = 20.0; // amount trimmed radially (80 -> 60)
const double innerTrdX1_new = innerTrdX1 + (innerTrdX2 - innerTrdX1) * (dY / 80.0);
// innerTrdX1_new = 24.202 (after substitution)
```

4. Increase the inner sector radius by 20 cm:

```
const double sectorRmin = 86.0;
```

Strip placement. Strip centers fill the trapezoid uniformly from the inner to the outer radius with step `stripY`; the first center is at 0.5 `stripY`. The transverse coordinate X scales linearly along the trapezoid height:

```
double Yshift = stripY/2. + (id - 1) * stripY; // distance from the inner edge along radius
double X = innerTrdX1_new + (Yshift - stripY/2.) * (innerTrdX2 - innerTrdX1_new) / innerTrdY;
```

Result. After the changes, each sector contains 48 strips; the geometry is consistent (the inner base and radial size are recalculated), and the sector's inner radius is updated. The corrected version is shown in Fig. 4.

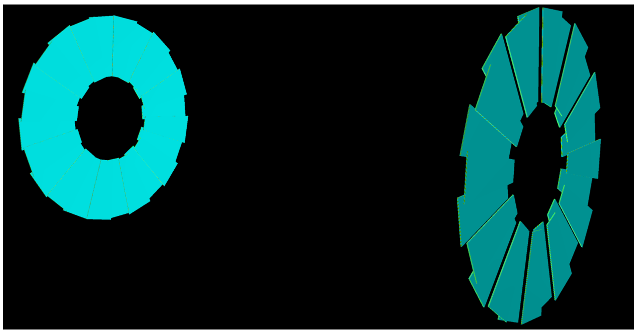

Figure 3: First generated ETOF sector version.

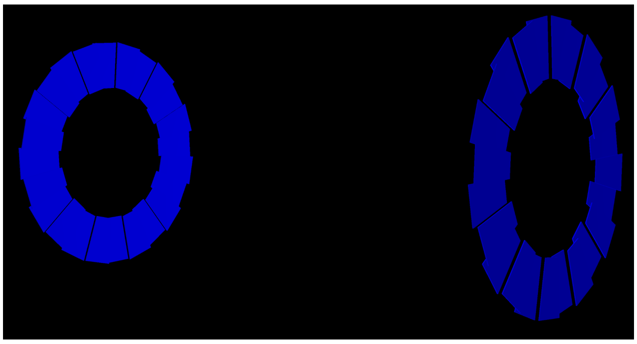

Figure 4: Corrected ETOF sector after strip reduction and geometry recalculation.

5.3 Integrating ETOF into MPD

The next step is to integrate ETOF into the full MPD geometry and check for overlaps. In the $Z = \pm 325$ cm configuration, ETOF was connected via `geometry_stage1.C` and the `runMC.C` macro was executed. TEve visualization and the standard `gGeoManager->CheckOverlaps()` procedure were used for validation [12, 13]. No overlaps were found for the volumes considered (see Fig. 5).

Note that not all mechanical elements (mounts, cables, gas lines, etc.) are included at this stage. Adding them to the geometry may require further placement adjustments of the ETOF modules.

6 Occupancy Studies

6.1 Preparation

To verify geometry functionality, the detector was "shot" with a Monte Carlo generator and *points* generation was checked. Initially, no ETOF *points* were produced; after updating the `tof` and `etof` configuration files, points were generated correctly.

From the geometry macro: two endcaps with 12 sectors each, 48 strips per sector, and readout from both strip ends. In total, $24 \times 2 \times 48 = 2304$ readout channels.

For basic checks of the geometry and reconstruction algorithms, we first used the simple `BOX` generator producing uniform distributions in angles and momenta. This allows assessing the baseline detector response and hit registration without a physics collision model.

For realistic particle distributions and *occupancy* plots, we used `UrQMD` (Ultra-relativistic Quantum Molecular Dynamics) [14]. The generator simulates heavy-ion collisions using a hadronic cascade with nucleons, resonances, and mesons, including production, scattering, and decay processes. We used Bi+Bi events at $\sqrt{s_{NN}} = 9$ GeV, within the NICA operation range.

We focused mainly on central collisions, which reach the highest energy density and the largest multiplicities of secondaries. This probes ETOF under the most demanding conditions

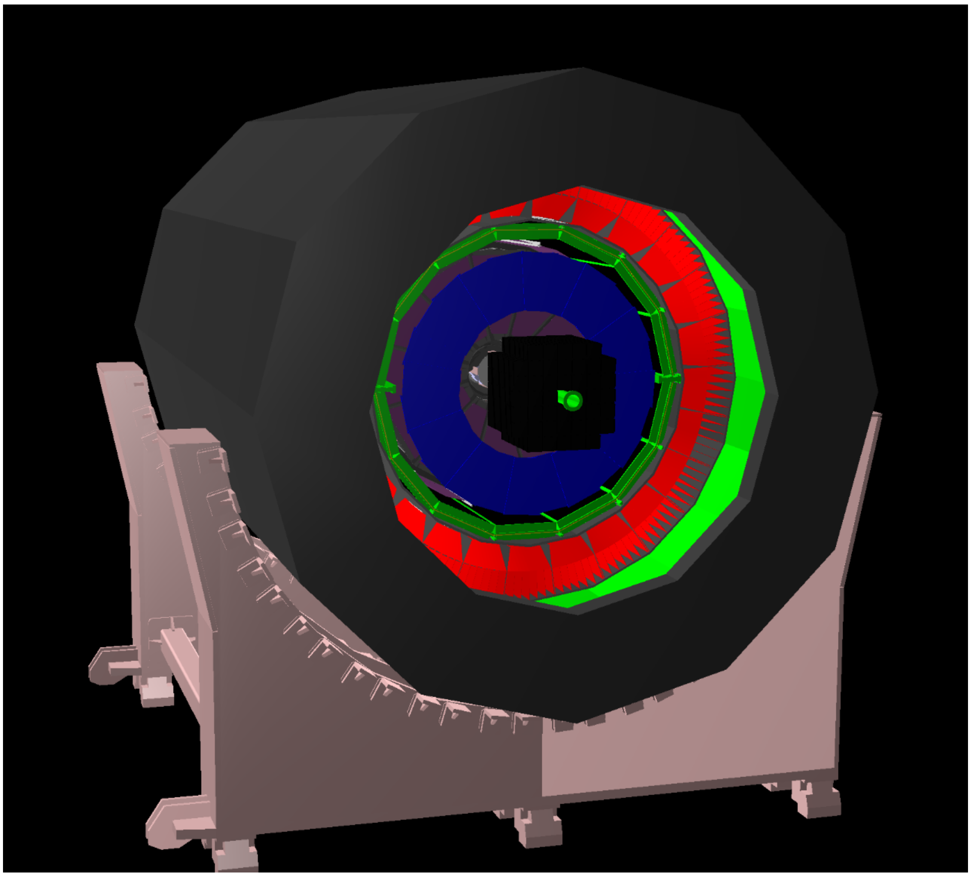

Figure 5: MPD with installed ETOF ($Z = \pm 325$ cm configuration).

and provides an upper bound on the expected *occupancy*. A `.root` file with *points* is produced after the run.

6.2 Occupancy calculation

Occupancy is the average fraction of readout channels that register at least one activation in an event. It quantifies the fraction of channels busy with signals from particle detection.

Since each ETOF strip has two readout channels, the total number of channels is

$$N_{\text{channels}} = N_{\text{sectors}} \times N_{\text{strips per sector}} \times 2.$$

For the current configuration, $N_{\text{sectors}} = 24$ and $N_{\text{strips}} = 48$, hence $N_{\text{channels}} = 2304$. These channels are uniformly distributed over 48 radial rings, each containing 48 channels. The calculation uses the detector geometry parameters: minimum radius $r_{\text{min}} = 86.0$ cm and radial step $\Delta r = 1.25$ cm.

The `DrawOccupancyMany.C` macro reads *points* from the `mpdsim` tree of ROOT files obtained after the Monte Carlo generation. Each point corresponds to a particle interaction within a sensitive element. For each event:

1. Extract (x,y) coordinates of all *points* from the `ETOFPoint` array.
2. Compute the radius $r = \sqrt{x^2 + y^2}$ and angle $\varphi = \arctan 2(y,x)$.

3. Discretize radius into 48 rings (step Δr) and angle into 48 equal sectors ($\Delta\varphi = 2\pi/48$), matching the channel segmentation.

4. Treat each unique (r_i, φ_j) pair in the event as an *activated channel.*

5. For each ring, count the number of unique activated channels N_i^{evt}.

After processing all events, compute the average channel occupancy:

$$\text{Occ}(R_i) = \frac{\langle N_i^{\text{evt}} \rangle}{N_{\text{channels in ring}}}.$$

This definition reflects the average activation probability per channel for a given particle flux. In this version, the calculation is performed on *points*, i.e., prior to *hit* reconstruction.

Results and visualization. The macro automatically produces two plots:

- ▷ the distribution of interaction points on the XY plane;
- ▷ the radial *occupancy* profile, i.e., the average channel occupancy vs. radius.

Figure 6 shows the point distribution over the detector surface, and Fig. 7 shows the computed *occupancy* vs. radius for UrQMD events.

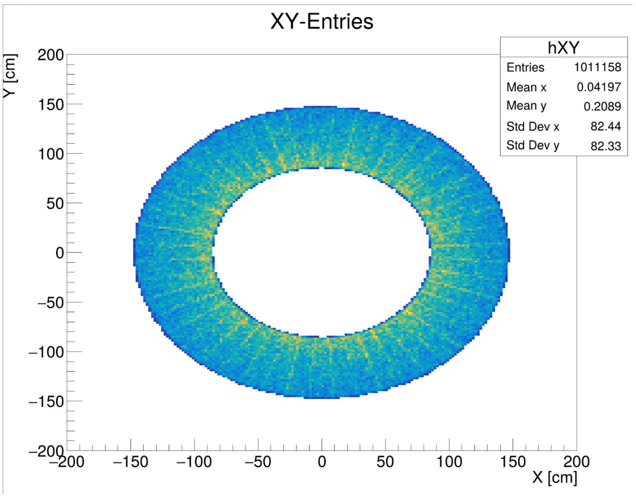

Figure 6: Distribution of *points* over the ETOF surface. UrQMD generator (800 events).

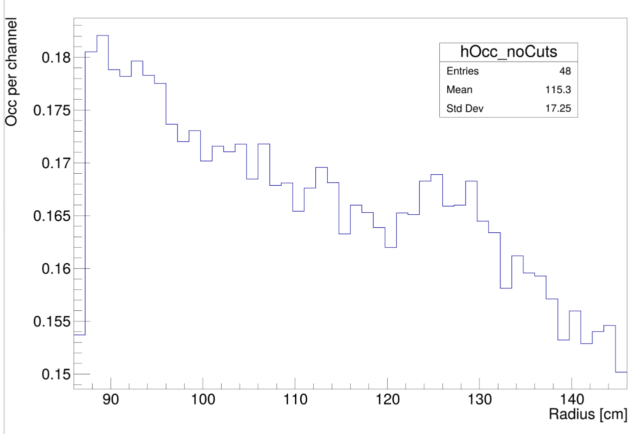

Figure 7: *Occupancy* vs. radius. UrQMD generator (800 events).

7 Sealed MRPC Module Prototype

7.1 Overview

As a practical part of the work, a laboratory MRPC module prototype was built following sealed-chamber designs from the literature [15], taking into account technological notes from [11]. The goal was to practice assembling a multi-gap chamber (5 gas gaps), frame layout, glass cutting and preparation, and resistive-layer application.

The frame and overall assembly were modeled in Autodesk Inventor (see Figs. 8 and 9). Photos of the assembly process and the completed prototype are shown in Figs. 10 and 11.

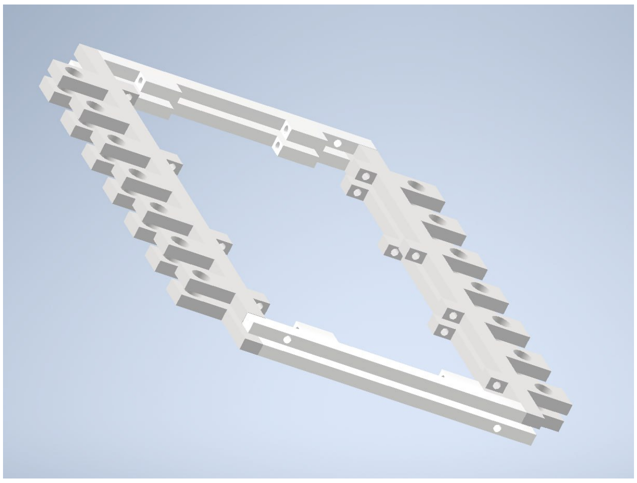

Figure 8: 3D model of the sealed MRPC frame.

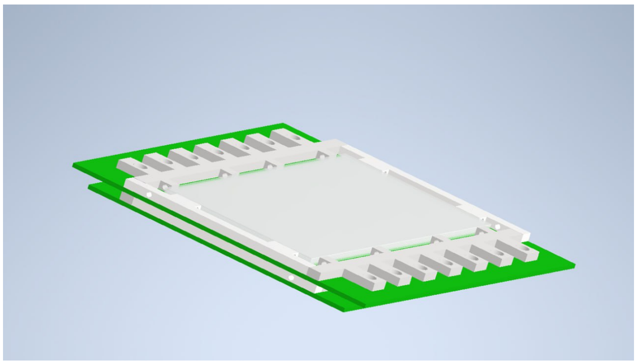

Figure 9: 3D model of the sealed MRPC (overall view).

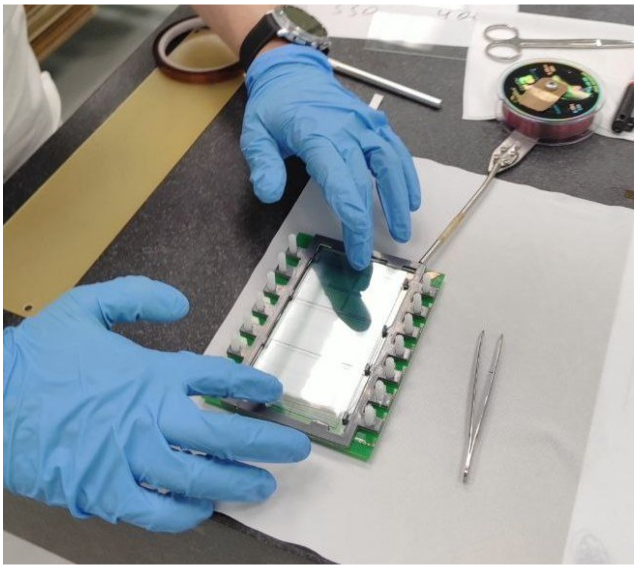

Figure 10: Assembly process of the sealed MRPC prototype.

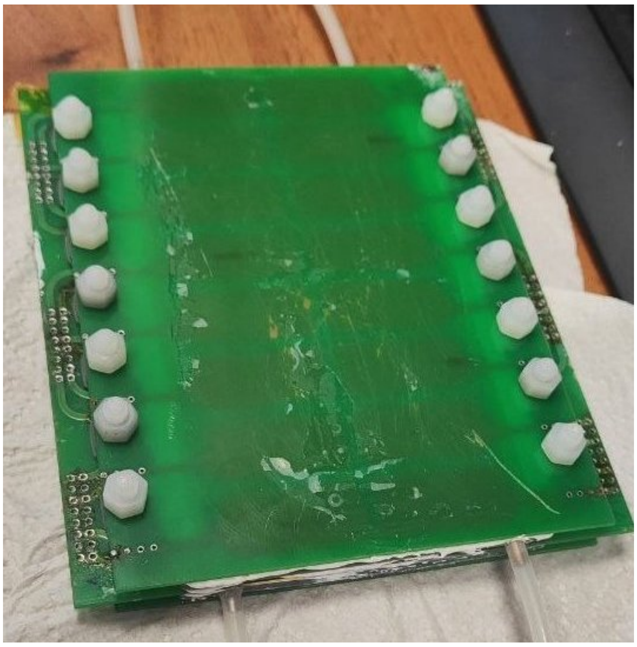

Figure 11: Completed sealed MRPC prototype.

7.2 Assembly procedure

The assembly proceeds in several stages:

1. Frame preparation (finishing, fit control) and glass test-fitting.

2. Application of the resistive layer to the high-voltage glass, drying, resistance measurement (target value of order 10 MΩ).

3. Building the **bottom volume**: glue the frame, place the HV glass with the resistive layer, lay the nylon monofilament (first gap), place a thin glass sheet; repeat “line + glass” to obtain 5 gaps.

4. The **top volume** is formed analogously.

7.3 Sealing and test status

At the assembly stage, sealing was provided by a *sealant* (sufficient for initial mechanical/gas tests). Electrical tests and connection to readout electronics *were not performed.*

8 Conclusion

The ETOF geometry was adapted in `mpdroot`. The inner part of the sector was shortened (reducing the number of strips to 48 per sector) with recalculated dimensions and placement; the module positions were refined ($Z = \pm 325$ cm). The MPD+ETOF assembly was validated (no overlaps), and the infrastructure for a preliminary *occupancy* calculation based on *points* was implemented.

The obtained geometric parameters and *occupancy* profiles serve as input for the subsequent transfer of the ETOF geometry to the ACTS surface representation and for the validation of track reconstruction within that framework.

Additionally, a laboratory prototype of a sealed MRPC module was manufactured. Tests were not performed and are planned for future work.

Acknowledgements

The author thanks the MPD Software Development team for consultations and support, and the scientific supervisor for setting the task and discussing the results.

References

[1] *The Multi-Purpose Detector (MPD) at NICA: Conceptual Design Report*. Tech. rep. Accessed 2025-10-13. Joint Institute for Nuclear Research (JINR), 2020. URL: https://mpd.jinr.ru/wp-content/uploads/2023/11/MPD_CDR_en.pdf.

[2] *Time Projection Chamber for MPD at NICA: Technical Design Report*. Tech. rep. Accessed 2025-10-13. MPD Collaboration, JINR, 2019. URL: https://mpd.jinr.ru/wp-content/uploads/2023/11/TpcTdr-v07.pdf.

[3] *MPD Time-of-Flight (TOF) System: Technical Design Report, Version 3.02*. Tech. rep. Accessed 2025-10-13. MPD Collaboration, JINR, 2021. URL: https://mpd.jinr.ru/wp-content/uploads/2023/11/TDR_TOF_MPD_v3_02-14_04_2021.pdf.

[4] *The Report on Project "MPD. Multi-Purpose Detector"*. Tech. rep. Accessed 2025-10-13. Joint Institute for Nuclear Research (JINR), 2025.

[5] V. Abgaryan, R. Acevedo Kado, S. V. Afanasyev, et al. "Status and Initial Physics Performance Studies of the MPD Experiment at NICA". In: *European Physical Journal A* 58.140 (2022). Accessed 2025-10-19. DOI: 10.1140/epja/s10050-022-00750-6. URL: https://link.springer.com/article/10.1140/epja/s10050-022-00750-6.

[6] Xiaocong Ai, Corentin Allaire, Noemi Calace, Angéla Czirkos, Markus Elsing, et al. "A Common Tracking Software Project". In: *Computing and Software for Big Science* 6.1 (2022), p. 8. DOI: 10.1007/s41781-021-00078-8. URL: https://cds.cern.ch/record/2775922/files/document.pdf.

[7] *ACTS Documentation*. Accessed 2025-10-13. URL: https://acts.readthedocs.io/en/latest/.

[8] Are Strandlie and Rudolf Frühwirth. "Track and Vertex Reconstruction: From Classical to Adaptive Methods". In: *Reviews of Modern Physics* 82 (2010), pp. 1419–1458. DOI: 10.1103/RevModPhys.82.1419. URL: https://link.aps.org/doi/10.1103/RevModPhys.82.1419.

[9] E. Kryshen and MPD Collaboration. *Endcap Detectors for MPD at NICA*. Indico slides / project reports. Overview talks on endcap systems; accessed 2025-10-13. 2020. URL: https://indico.jinr.ru/.

[10] *MPD Experiment Official Website*. Accessed 2025-10-13. URL: https://mpd.jinr.ru/.

[11] V. A. Babkin. "Time-of-Flight Particle Identification System of the Multi-Purpose Detector (MPD)". Doctoral thesis (in Russian); accessed 2025-10-13. PhD thesis. Joint Institute for Nuclear Research (JINR), 2020. URL: https://indico.jinr.ru/event/1674/contributions/10851/attachments/8608/12939/%D0%A2%D0%B5%D0%BA%D1%81%D1%82%20%D0%B4%D0%B8%D1%81%D1%81%D0%B5%D1%80%D1%82%D0%B0%D1%86%D0%B8%D0%B8_v1_0_2_S.pdf.

[12] *ROOT Data Analysis Framework*. Accessed 2025-10-13. URL: https://root.cern/.

[13] *ROOT EVE: Event Visualization Environment (API Documentation)*. Accessed 2025-10-13. CERN. 2024. URL: https://root.cern/doc/v636/group__TEve.html.

[14] S. A. Bass, M. Belkacem, M. Bleicher, M. Brandstetter, L. Bravina, et al. "Microscopic Models for Ultrarelativistic Heavy-Ion Collisions". In: *Progress in Particle and Nuclear Physics* 41 (1998), pp. 225–370. arXiv: nucl-th/9803035. URL: https://arxiv.org/abs/nucl-th/9803035.

[15] H. Chen et al. *Development of Sealed MRPC with Extremely Low Gas Flow*. Preprint/Conference. Prototype sMRPC; accessed 2025-10-13. 2020. URL: https://inspirehep.net/literature/1785170.